# Evaluation of the next generation gamma imager

K. Amgarou, T. Timi, N.B. de Lanaute, Frédérick Carrel, Vincent Schoepff, Hermine Lemaire, Mehdi Gmar, R. Abou Khalil, S. Dogny, T. Varet, et al.

# Evaluation of the next generation gamma imager

Khalil Amgarou, Tebug Timi, Nicolas Blanc de Lanaute
CANBERRA, 1 rue des Hérons, Saint Quentin-en-Yvelines, F-78182, France. (phone number: +33139485713, e-mail: khalil.amgarou@canberra.com

Frédérick Carrel, Vincent Schoepff, Hermine Lemaire, Mehdi Gmar
CEA, Sensors and Electronic Architectures, Gif-sur-Yvette, F-91191, France

Roger Abou Khalil, Stéphane Dogny, Thierry Varet
AREVA, place Jean Millier, Paris La Défense, F-92084, France

Audrey Patoz, Philippe Talent, Nabil Menaa
CANBERRA, 1 rue des Hérons, Saint Quentin-en-Yvelines, F-78182, France

## Abstract

Towards the end of their life-cycle, nuclear facilities are generally associated with high levels of radiation exposure. The implementation of the ALARA principle requires limiting the radiation exposure of the operating people during the different tasks of maintenance, decontamination and decommissioning. CANBERRA's latest involvement in the provision of nuclear measurement solutions has led, in the framework of a technology transfer agreement with CEA LIST, to the development of a new generation gamma imager. The latter, which is designed for an accurate localization of radioactive hotspots, consists of a pixilated chip hybridized to a 1 mm thick CdTe substrate to record photon pulses and a coded mask aperture allowing for background noise subtraction by means of a procedure called mask/anti-mask, which greatly contributes to the reduced size and weight of the gamma imager as gamma shielding around the detector is less required. The spatial radioactivity map is automatically superimposed onto a pre-recorded photographic (visible) image of the scene of interest. In an effort to evaluate the performances of the new gamma imager, several experimental tests have been performed on a industrial prototype to investigate its detection response, including photon sensitivity and angular resolution, over a wide energy range (at least from 59 keV to 1330 keV). The impact of the background noise was also evaluated together with some future features like energy discrimination and parallax correction. This paper presents and discusses the main results obtained in the above experimental study. A comparison with Monte Carlo simulations using the MCNP code is provided as well.

## Keywords

Gamma imaging, radioactive hotspots, coded mask aperture, CMOS pixilated readout chip

## I Introduction

REAL-TIME tracking of radioactive hotspots is of prime concern in nuclear facilities such as nuclear power plants or high-energy research accelerators, especially at the end of their life-cycle where the operational radiological protection is permanently needed during the different tasks of maintenance, decontamination and decommissioning. For this purpose, gamma

imaging systems, firstly introduced by Anger in the 1960s [1], can provide the best solution since they enable rapid remote measurements leading to significant reductions of doses received by the nuclear workers as well as operation times and costs. Gamma imagers are also highly valuable in medicine [2], for detecting early stage tumors, and in astronomy [3] for revealing relevant information about black holes or neutron stars. However, the associated equipments for these application areas are generally too bulky, heavy and complex to be used for routine monitoring in nuclear facilities.

A first attempt to develop a compact, light and easy-to-use gamma imager was carried out in the 1990s by CEA LIST[1]. The outcome of this effort was the CARTOGAM instrument [4], widely commercialized by CANBERRA during the last decade. It consists of a mature technology combining an inverted double-cone collimator (i.e., two right circular cones placed apex to apex) with a pinhole aperture, a scintillation crystal CsI/Tl[2], a multichannel image intensifier and a CCD[3] camera. The whole (except the pinhole aperture) is fully shielded within a Denal[4] cylindrical head of 80 mm diameter and 414 mm length to avoid the influence of high background radiation.

As a recall, a basic photographic camera simply consists of a light-opaque box with a single pinhole on one side and through which the light coming from an object is projected as an inverted image on the opposite side inside the box. CARTOGAM, which is based on this basic principle applied to gamma detection, is able to generate a picture of the spatial radioactivity map and to automatically represent it superimposed onto a photographic image of the scene of interest. This image is recorded with the CCD camera placed behind the CsI/TI crystal, which is fully transparent to visible photons, using a removable lens. Nevertheless, even it is still demonstrating good performances at severe irradiation conditions, its weight of ~18kg is sometimes a real constraint.

Recently, in the framework of a technology transfer agreement, CEA LIST and CANBERRA have been working on a new generation of miniaturized gamma imagers [5]–[8] with improved characteristics in terms of portability, sensitivity and angular resolution, using an advanced photon detector based on a pixilated readout CMOS[5] chip, called Medipix 2 [9], a coded mask aperture [10] and a mini photo-camera. The coded mask, which is an efficient generalization of the pinhole imaging principle [11], contains a binary array or pattern of open and closed circular cells, uniformly distributed under a particular sequence. This design allows a direct background noise subtraction by means of a procedure called mask/anti-mask, which greatly contributes to the reduced size and weight of the gamma imager as gamma shielding around the detector is less required.

The present paper summarizes the main specifications of a first industrial prototype of the new generation gamma imager and reports the results of an experimental and theoretical study. These results are extremely helpful in defining the main future features of the final commercial product, expected for the end of this year.

---

1 CEA is the French Commission for Alternative and Atomic Energies (Commissariat à l'énergie atomique et aux énergies alternatives) and LIST isits Laboratory for System and Technology Integration (Laboratoire d'Intégration des Systèmes et des Technologies).

2 Thallium doped cesium iodide

3 Charge-Coupled Device

4 An alloy metal with 95% tungsten, 2.5% nickel and 2.5% iron.

5 Complementary Metal Oxide Semiconductor

## Main Specifications

Fig. 1 presents the first industrial prototype of the new generation gamma imager, with a weight below 2 kg and 80×80×150 $mm^3$ external dimensions. As stated in the previous section, it includes a Medipix 2 based photon detector (active area of ∼2 $cm^2$), a coded mask aperture and a mini photo-camera.

The Medipix 2 chip is hybridized to a 1 mm thick CdTe[6] substrate and consists of 256 ×256 identical elements or pixels, working as a single photon counter for positive or negative input charge signals. Due to its high atomic number and density (Z = 48.52, $\rho$ = 5.32 g $cm^{-3}$) compared to Si and GaAs,CdTe shows a good photon sensitivity over a large energy range, from ∼4eV up to several *MeV* [12]. Each pixel contains around 500 transistors and occupies a surface of 55×55 $\mu m^2$. A 20 mm width octagonal opening connects the detector and the preamplifier input via bump-bonding.

The preamplifier feedback provides compensation for detector leakage current on a pixel by pixel basis. Two identical pulse height discriminators are used to create a digital pulse if the preamplifier output falls within a defined energy window. The whole digital pulses are then counted with a 13-bit pseudo-random counter. An individual 8-bit configuration register also offers the possibility of masking, test-enabling and 3-bit threshold adjust for each discriminator.


**Fig. 1** First industrial prototype of the new generation gamma imager.

---

6 Cadmium telluride.

According to the photon detector shape and the specific mathematical rules described in Ref. [10], the following three square Denal coded masks were designed (see Fig. 2):

- M13–2 with a rank[7] 13 and 2 mm thickness,
- M7–4 with a rank 7 and 4 mm thickness, and
- M7–8 with a rank 7 and 8 mm thickness.

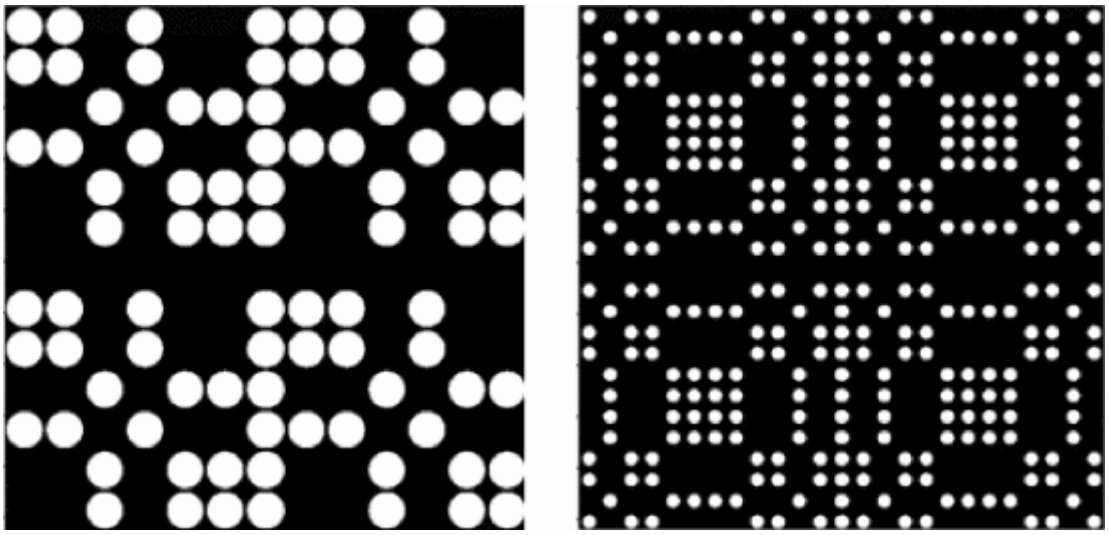

**Fig. 2** Coded masks with rank 7 (on the left) and rank 13 (on the right).

The maximum field-of-view (FOV) of the photon detector along the horizontal (*x*-axis) and vertical (*y*-axis) axes is 47°×47° while that of the photo-camera is 56°×38°. The latter is located diagonally with respect to the mask centre, as shown in Fig. 1, at practically 39 mm (i.e., $x = 32$ mm and $y = 22$ mm) distance.

At environments with high background radiation, the mask/anti-mask procedure may be applied using two consecutive measurements: one with the mask in its normal position and another with the mask in the "anti-mask" position (achieved by rotating the mask 90° from its normal position). By subtracting the readings of both measurements, it is possible to fully compensate for the background contribution.

---

7 Number of open circular cells in the basic pattern.

## II Testing and Evaluation

### A. Parallax Correction

Generally, due to the fact that the photon detector and the photo-camera have different FOVs, a parallax error may take place as observed in Fig. 3. This effect can be systematically corrected by providing the actual distance of the considered radioactive source or hotspot. This correction is always applied by default although the parallax error has a low influence when the source-to-detector distance is above 2 m.

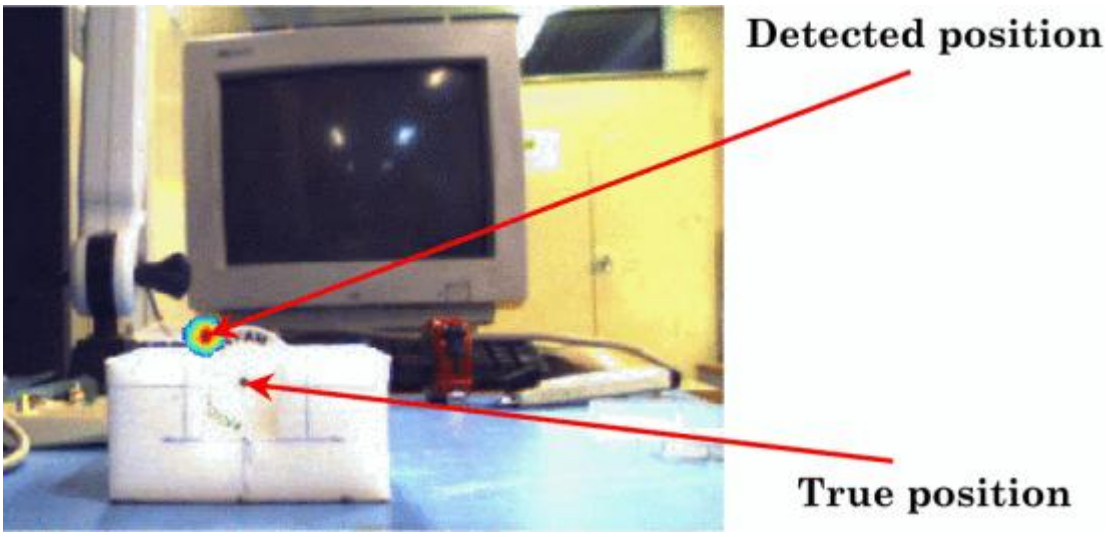


**Fig. 3** Example of a parallax error due to the fact the photon detector and the photo-camera have different FOVs.

### B. Gamma Imaging Sensitivity

The gamma imaging sensitivity has been studied with the following three radioactive sources: $^{241}Am$ (emitted $\gamma$ rays of 59 keV energy and $72.7\times10^6$ Bq activity), $^{137}$Cs (662 keV and $25.6\times10^6$ Bq) and $^{60}$Co (1173 keV, 1332 keV and $36.6\times10^6$ Bq). The source-to-detector distance was fixed to 1 meter whereas the acquisition time was varied between 1 second and 10 minutes. Fig. 4 gives an example of how the measurement time affects the estimation of the sought spatial radioactivity map in the case of $^{60}$Co using the mask M7–8. All the results obtained in terms of the qualitative minimum time, Tmin, needed to locate the radioactive sources with sufficient image resolution and ambient dose equivalent rate are summarized in Table I.

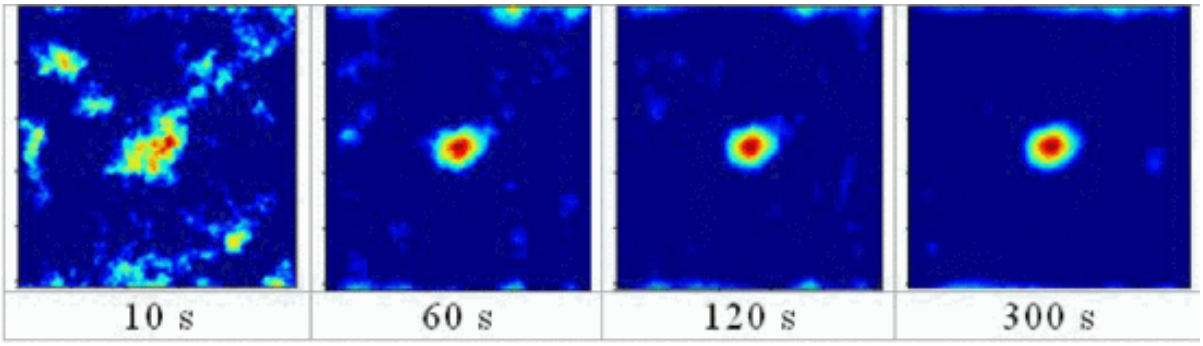


**Fig. 4** Estimation of the spatial radioactivity map vs. measurement time in the case of $^{60}$Co using the mask M7–8.

| | $T_{min}$ | | | Ambient dose equivalent rate | |
|---|---|---|---|---|---|
| | M13-2 | M7-4 | M7-8 | Reference | Estimated |
| $^{241}$Am | ~ 3 s | ~ 1 s | ~ 2 s | 0.25 µSv/h | 0.22 µSv/h |
| $^{137}$Cs | - | ~ 60 s | ~ 30 s | 2.5 µSv/h | 2.5 µSv/h |
| $^{60}$Co | - | ~ 120 s | ~ 40 s | 12.3 µSv/h | 13.23 µSv/h |

**TABLE I** Sensitivity Study Results

### C. Angular Resolution

One of the key requirements in gamma imaging is the ability to track several radioactive sources at the same time. The angular resolution is the most convenient parameter to define the distinction limit, $\theta_{min}$, between two small and adjacent radioactive sources. According to Fig. 5, $\theta_{min}$ depends on the diameter, $d$, of the open cells on the coded mask and the distance, $D$, between the mask and the detector. It can also be experimentally estimated from vertical or horizontal distribution of the measured counts at photon detector, as illustrated in Fig. 6, taking into account the associated the FWHM[8] and the detection field-of-view (FOV).

---

8 Full width at half maximum

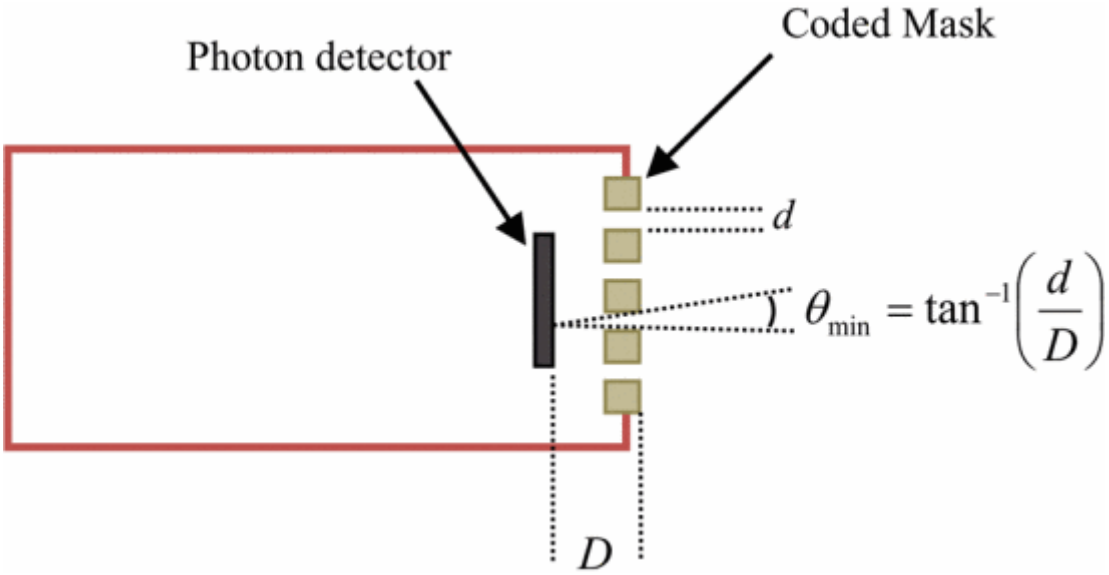


**Fig. 5** Angular resolution of a gamma of the new generation gamma imager.

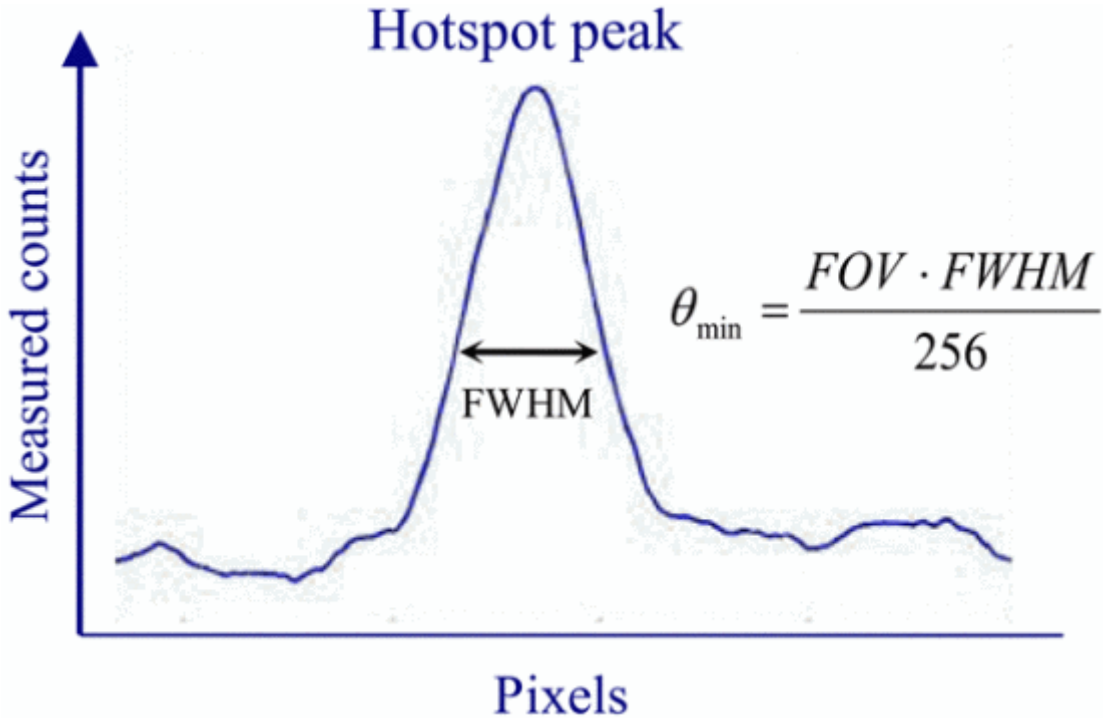


**Fig. 6** Vertical or horizontal distribution of the measured counts at photon detector (of 256×256 pixels). The FWHM is determined by applying a Gaussian fit to the hotspot peak.

| | Calculated | Measured | | |
|---|---|---|---|---|
| | | $^{241}$Am | $^{137}$Cs | $^{60}$Co |
| M13-2 | 2.5° | 2.13° | - | - |
| M7-4 | 6.4° | 6.13° | 6.09° | 5.91° |
| M7-8 | 5.8° | 5.95° | 6.00° | 6.23° |

**TABLE II** Angular Resolution

Both methods are close to each other to within 15% (see Table II). Fig. 7 shows some results obtained with M13–2 and M7–4 coded masks and three different $^{241}$Am radioactive sources (Sl: $1.26\times10^{9}$ Bq; S2: $2.90\times10^{9}$ Bq; S3: $3.09\times10^{9}$ Bq).

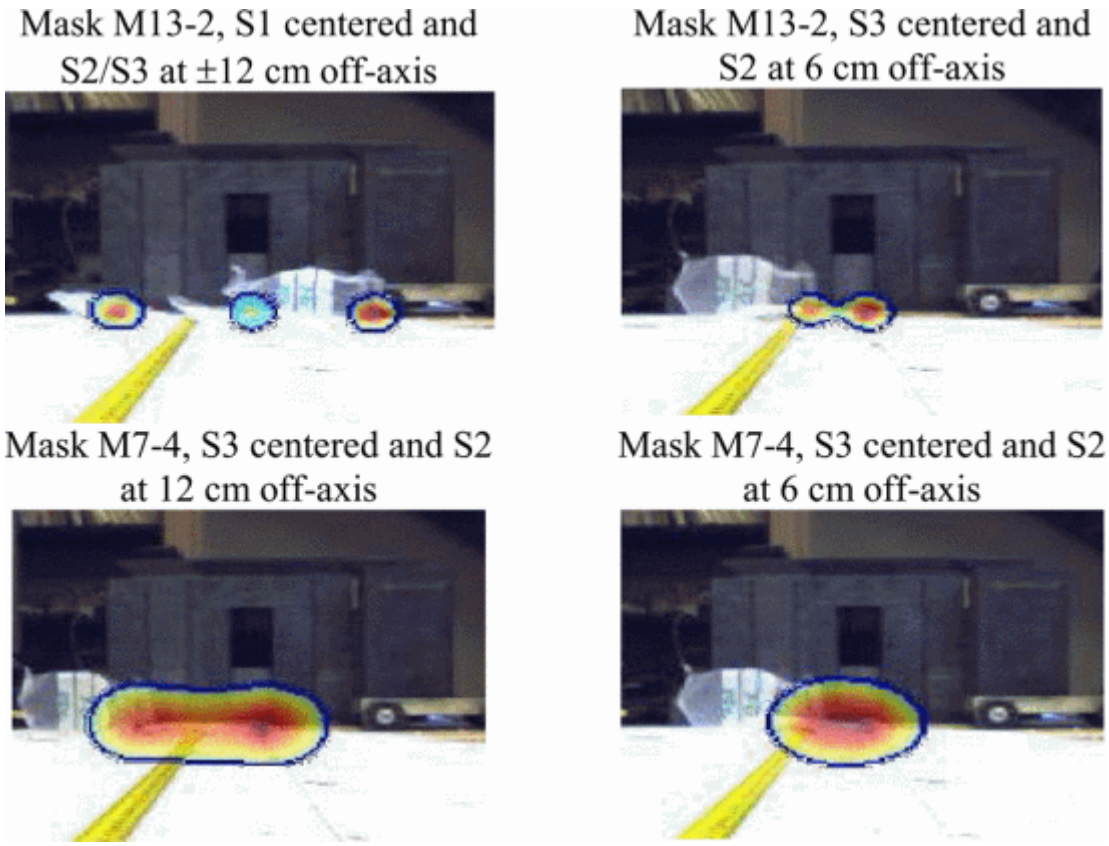


**Fig. 7** Example of multi-source tracking with new generation gamma imager.

**D. Response Linearity**

Fig. 8 presents the measured count rate at the hotspot peak as a function of the ambient dose rate in the case of $^{137}$Cs using the mask M7–4. It can be seen in this figure that the response of the photon detector is linear up to 50 $\mu$Sv/h.

It should be pointed out that the upper value of 50 $\mu$Sv/h is only due to specific experimental restrictions when using a $^{137}$Cs radioactive source with limited activity ($25.6\times10^{6}$ Bq). Indeed, previous works, carried out with the original research prototype (developed by CEA LIST) and a highest activity ($\sim10^{13}$ Bq) of the $^{137}$Cs radioactive source [8], have shown that the response linearity of the photon detector even reached a maximum of 5 Sv/h and we except that it can easily exceed this value.

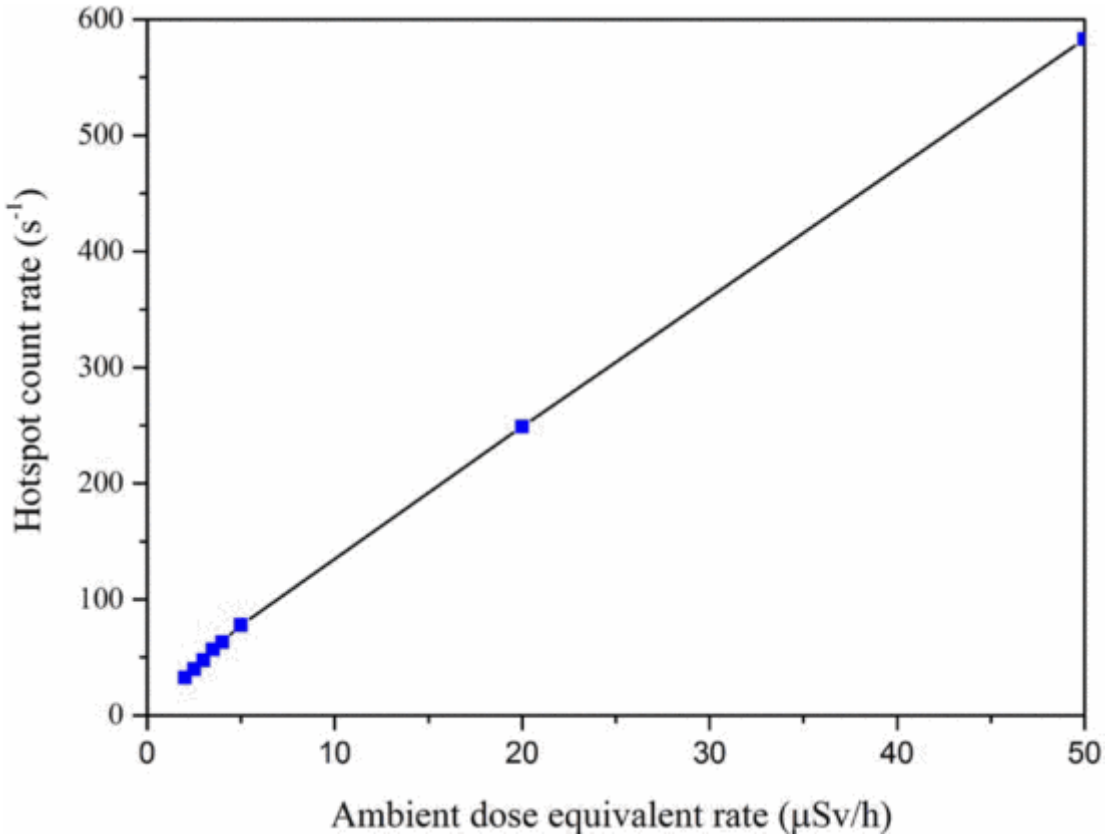


**Fig. 8** Measured count rate at the hotspot peak as a function of the ambient dose rate in the case of $^{137}$Cs using the mask M7–4.

**E. Monte-Carlo Simulations**

Several Monte-Carlo simulations of the industrial prototype described in Section II and the different masks were equally carried out by use of the MCNPX code [13]. The chosen model, as illustrated in Fig. 5, consists of an aluminum box, the coded mask aperture, and the photon detector.

Figures 9, 10 and 11 provide the measured and MCNPX response profiles of the new generation gamma imager with the three coded masks to the $^{241}$Am radioactive sources as a function of the radioactive source off-axis position.

The agreement found is good and both the experimental and simulated results make evident that when the off-axis position of the radioactive source increases the response of the photon detector decreases.

Moreover, the self-attenuation of the incident X-rays with low energies, such is the case of the $^{241}$Am radioactive source, is more accentuated with the thicker mask (i.e., M7–8) but this effect is less important in the case of the M7–4 coded mask compared to M13–2. The latter, even having the lowest thickness, the small diameter of its open cells ultimately penalizes its response at the central position whereas the ones of M7–4 and M7–8 are quite similar.

Conversely, the self-attenuation effect is fairly negligible for the $^{137}$Cs and $^{60}$Co radioactive sources, emitting photons that are higher in energy than those of $^{241}$Am.

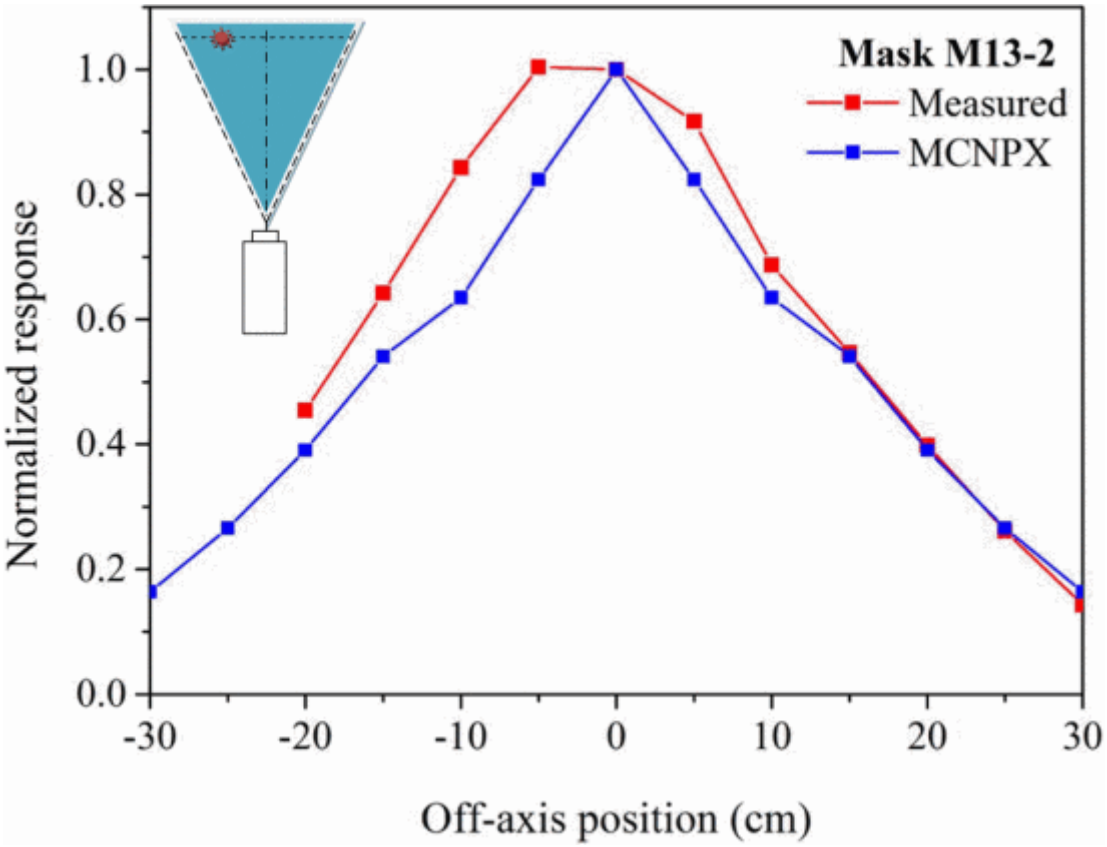


**Fig. 9** Measured and MCNPX response profiles of the new generation gamma imager with the coded mask M13–2 to the $^{241}$Am radioactive source as a function of the radioactive source off-axis position.

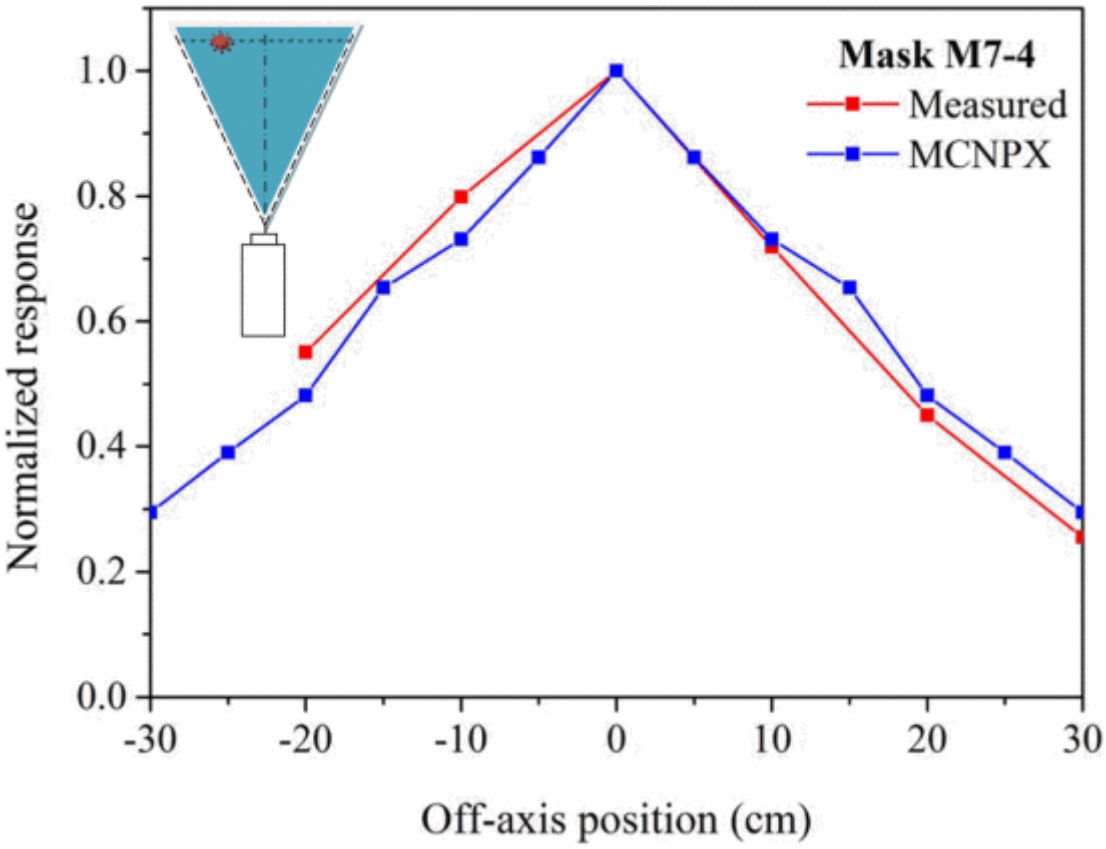

**Fig. 10** Measured and MCNPX response profiles of the new generation gamma imager with the coded mask M7–4 to the $^{241}$Am radioactive source as a function of the radioactive source off-axis position.

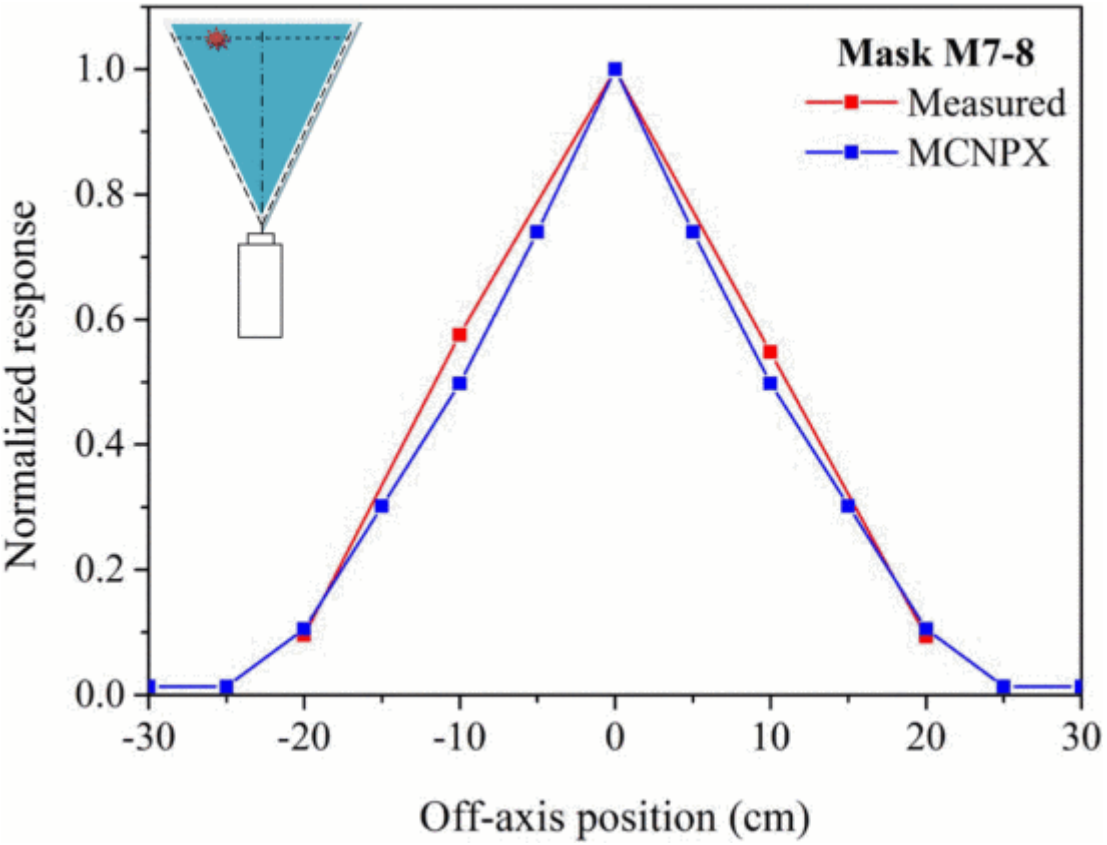


**Fig. 11** Measured and MCNPX response profiles of the new generation gamma imager with the coded mask M7–8 to the $^{241}$Am radioactive source as a function of the radioactive source off-axis position.

**F. Energy Discrimination**

Medipix 2 is able to roughly discriminate between the energy of incident photons by filtering the registered cluster

- An upper threshold of 2.5 to select only incident photon energies below 300 keV.
- An interval of [2.5–4.5] to select only incident photon energies between 300 keV and 800 keV.
- A lower threshold of 4.5 to select only incident photon energies above 800 keV.

To test these filtering criteria both the $^{241}$Am and $^{60}$Co radioactive sources cited in Section II-B were placed simultaneously in front of the new generation gamma imager with the coded mask M7–8 and we tried to visualize or hide each one of them on the captured visible image by selecting the appropriate cluster sizes. The results obtained are presented in Fig. 12. We can observe in this figure that by filtering the cluster sizes below 2.5 only the $^{241}$Am radioactive source is visualized while hiding that of $^{60}$Co. The opposite effect occurs (i.e., visualizing the $^{60}$Co radioactive source and hiding that of $^{241}$Am) when all the cluster sizes above 4.5 are considered.

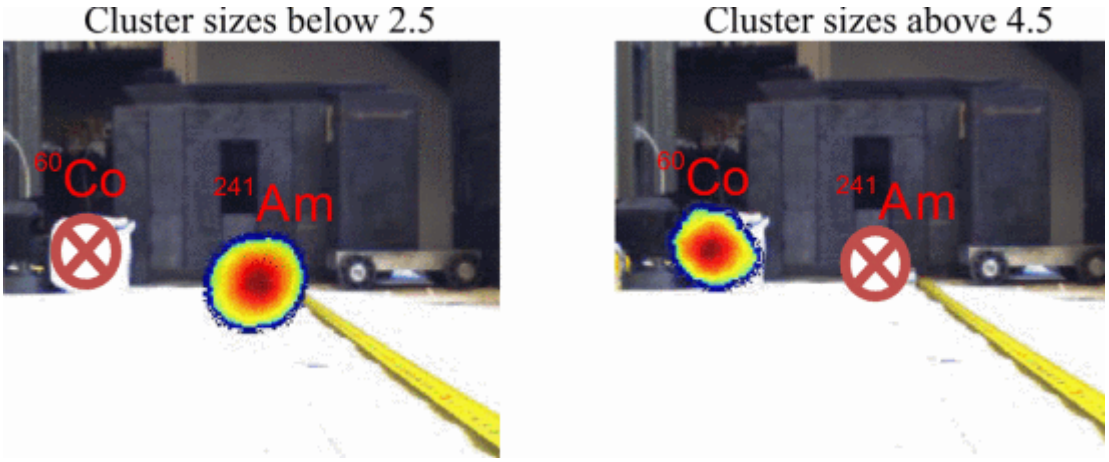


**Fig. 12** Energy discrimination by filtering the cluster sizes.

### G. Background Noise

The background noise was studied by putting the S1 radioactive source at 100 cm distance in front of the coded mask M7–4 and S3 near the prototype but out-of-field of the photon detector. Consequently, the parasite counts due to the presence of S3 have considerably increase but owing to the unfolding method used an optimum signal-to-noise was found (only 5% difference was observed between measurements with and without S3).

## III Conclusions

The combination between the Medipix 2 pixilated readout chip and the mask/anti-mask technique greatly contributes to the reduced size ($80\times80\times150 mm^3$) and weight (<2 kg) of the new generation gamma imager. With this instrument, a radioactive source of few nSv/h can be visualized in less than one minute. The performances observed with the first prototype were encouraging and will be extremely helpful in defining the main future features of the final commercial product, expected for the end of this year.

### ACKNOWLEDGMENT

This work is partially supported by the BOOSTER project, which has received funding from the European Community's Seventh Framework Programme, in the research theme ‘Security’ (FP7-SECURITY/2007–2013), under the grant agreement number 242361.

## REFERENCES

[1] H. O. Anger, “Scintillation camera with multichannel collimators,” *J Nucl Med*, vol. 5, pp.515-531, 1964.
[2] J. Prekeges, *Nuclear Medicine Instrumentation*. Jones & Bartlett Publishers, 2010.
[3] G. Vedrenne, J.-L. Atteia, *Gamma-Ray Bursts: The brightest explosions in the Universe*. Springer/Praxis Books, 2009.
[4] O. Gal, C. Izac, F. Jean, F. Lainé, C. Lévêque, and A. Nguyen, “CARTOGAM – a portable gamma camera for remote localization of radioactive sources in nuclear facilities,” *Nucl. Instrum. Meth. A*, vol. 460, pp.138-145, 2001.

[5] O. Gal, M. Gmar, O. P. Ivanov, F. Lainé, F. Lamadie, C. Le Goaller, C. Mahé, E. Manach, V. E. Stepanov, "Development of a portable gamma camera with coded aperture," *Nucl. Instrum. Meth. A*, vol. 565, pp.233-237, 2006.
[6] M. Gmar, M. Agelou, F. Carrel and V. Schoepff, "GAMPIX: a new generation of gamma camera", *Nucl. Instrum. Methods Phys. Res. A*, Vol. 652, pp. 638-640, 2011.
[7] F. Carrel et al., "GAMPIX: A new gamma imaging system for radiological safety and Homeland Security Purposes," *Nuclear Science Symposium and Medical Imaging Conference (NSS/MIC)*, 2011 IEEE, DOI: 10.1109/NSSMIC.2011.6154706
[8] A. B. Khalil et al., "An evolution of technologies and applications of gamma imagers in the nuclear cycle industry," *Nuclear Science Symposium and Medical Imaging Conference (NSS/MIC)*, 2011 IEEE, DOI: 10.1109/ANIMMA.2011.6172915
[9] X. Llopart, R. Ballabriga, M. Campbell, L. Tlustos, W. Wong, "Medipix, a 65k programmable pixel readout chip for arrival time, energy and/or photon counting measurements," *Nucl. Instrum. Meth. A*, vol. 581, pp.485-494, 2007.
[10] S.R. Gottesman, E.E. Fenimore, "New family of binary arrays for coded aperture imaging," *Appl. Optics*, vol. 28, pp.4344-4352, 1989.
[11] R. H. Dicke, "Scatter-hole cameras for X-rays and gamma rays," *Astrophysics J.*, vol. 153, pp.L101-L106, 1968.
[12] S. del Sordo at al., "Progress in the Development of CdTe and CdZnTe Semiconductor Radiation Detectors for Astrophysical and Medical Applications," *Sensors*, vol. 9, pp.3491-3526, 2009.
[13] D. B. Pelowitz, ed., *MCNPX User's Manual*, *Version 2.6.0*, Los Alamos National Laboratory report LA-CP-07-1473, 2008.